VPS35 regulates developing mouse hippocampal neuronal morphogenesis by promoting retrograde trafficking of BACE1

Chun-Lei Wang[1], Fu-Lei Tang[1], Yun Peng[1], Cheng-Yong Shen[1], Lin Mei[1] and Wen-Cheng Xiong[1,2,*]

[1]Institute of Molecular Medicine and Genetics, and Department of Neurology, Medical College of Georgia, Georgia Health Sciences University, Augusta, GA 30912, USA
[2]Charlie Norwood VA Medical Center, Augusta, GA 30912, USA
*Author for correspondence (wxiong@georgiahealth.edu)

Biology Open 1, 1248–1257
doi: 10.1242/bio.20122451
Received 4th July 2012
Accepted 17th September 2012

Summary

VPS35, a major component of the retromer, plays an important role in the selective endosome-to-Golgi retrieval of membrane proteins. Dysfunction of retromer is a risk factor for neurodegenerative disorders, but its function in developing mouse brain remains poorly understood. Here we provide evidence for VPS35 promoting dendritic growth and maturation, and axonal protein transport in developing mouse hippocampal neurons. Embryonic hippocampal CA1 neurons suppressing Vps35 expression by *in utero* electroporation of its micro RNAs displayed shortened apical dendrites, reduced dendritic spines, and swollen commissural axons in the neonatal stage, those deficits reflecting a defective protein transport/trafficking in developing mouse neurons. Further mechanistic studies showed that Vps35 depletion in neurons resulted in an impaired retrograde trafficking of BACE1 (β1-secretase) and altered BACE1 distribution. Suppression of BACE1 expression in CA1 neurons partially rescued both dendritic and axonal deficits induced by Vps35-deficiency. These results thus demonstrate that BACE1 acts as a critical cargo of retromer *in vitro* and *in vivo*, and suggest that VPS35 plays an essential role in regulating apical dendritic maturation and in preventing axonal spheroid formation in developing hippocampal neurons.

Key words: VPS35, BACE1, Neural development

Introduction

Retromer, a protein complex initially identified in the yeast, is essential for retrograde transport of numerous membrane proteins from the endosomes to the *trans*-Golgi network (TGN) (Seaman, 2005; Bonifacino and Hurley, 2008). It contains two sub-protein complexes: one for the cargo-selection, and the other one for membrane deformation. The cargo-selective complex is a trimer of vacuolar protein sorting (Vps) proteins VPS35, VPS29, and VPS26 that sorts cargos into tubules for retrieval to the Golgi apparatus. The membrane deformation sub-complex consists of sorting nexin (SNX) dimers (Vps5p and Vps17p in yeast, and sortin nexins 1/3 or 5/6 in vertebrates) (van Weering et al., 2010; Seaman, 2005; Bonifacino and Hurley, 2008). A growing list of retromer cargos has been identified, including cation independent mannose 6-phosphate receptors (CI-MRP) (Arighi et al., 2004), wntless (a "receptor" for Wnt morphogens) (Belenkaya et al., 2008; Eaton, 2008; Franch-Marro et al., 2008; Pan et al., 2008; Port et al., 2008; Yang et al., 2008), Ced1 (a phagocytic receptor) (Chen et al., 2010), VPS10/sotilin family proteins, such as VPS10 in yeast (Iwaki et al., 2006), sortilin and sortilin-related receptor (SorL1 or SorCS1) in vertebrates (Canuel et al., 2008; Kim et al., 2010; Okada et al., 2010), and G-protein coupled receptors (e.g., Parathyroid hormone receptor and β2-adrenonergic receptor) (Feinstein et al., 2011; Temkin et al., 2011). Although retromer's endosome-to-Golgi retrieval function has been well established in yeast, *C. elegans*, *Drosophila*, and in mammalian cultured cells, its role in mouse just began to be understood.

Retromer is involved in the pathogenesis of neurodegenerative disorders, including Alzheimer's disease (AD) and Parkinson's disease (PD). The cargo-selective retromer proteins VPS35 and VPS26 are decreased in the postmortem hippocampus of AD patients (Small et al., 2005a). Genetic mutations of SorLA, a VPS10/sotililin family cargo of retromer, and Vps35 are identified in late-onset AD (Rogaeva et al., 2007; Willnow et al., 2010) and PD patients (Vilariño-Güell et al., 2011; Zimprich et al., 2011), respectively. These observations suggest that dysfunction of retromer complex may be a general risk factor for a growing list of neurodegenerative disorders. This view is further supported by recent studies using genetically mutant mouse models of retromer (Muhammad et al., 2008; Wen et al., 2011). Both Vps35 and Vps26 heterozygotes exhibit an increase in the production of amyloid β peptide (Aβ) (Muhammad et al., 2008; Wen et al., 2011), a 40–42 amino acid peptide derived from β- and γ-secretase cleavage of APP that is believed to be a major culprit of AD. In addition, Vps35 heterozygotes in Tg2576 mouse model of AD show earlier onset and enhanced AD-like neuropathology (Wen et al., 2011). Further mechanistic cellular studies suggest that loss of retromer function may alter the

trafficking of its cargos, including SorLA, APP, and BACE1, resulting in an increased Aβ production and enhanced AD neuropathology (Vieira et al., 2010; Willnow et al., 2010; Finan et al., 2011; Wen et al., 2011). However, the exact mechanism remains exclusive.

In order to study retromer's function, we have generated Vps35 mutant mouse, as VPS35 is a major component of retromer cargo recognition complex and is responsible for cargo recognition and the complex assembly (Seaman, 2005; Bonifacino and Hurley, 2008; McGough and Cullen, 2011). While hemizygous deletion of Vps35 gene in Tg2576 mouse model of AD leads to an earlier-onset AD-like phenotypes, homozygous died early during embryonic development (<E10, before neurogenesis) (Wen et al., 2011), preventing us from using this genetic model to address VPS35's function during mouse development. We thus used the RNA interference (RNAi) technology and the *in utero* electroporation assay to address this issue. Here, we showed that expression of miRNAs that suppress Vps35 expression in developing mouse CA1 neurons results in shortened apical dendrites, reduced dendritic spines, and swollen axons. These results suggest a role for VPS35/retromer in dendritic arborization or maturation and in preventing axonal spheroid formation during neonatal hippocampal development. We further investigated the underlying mechanisms and found that Vps35 depletion in hippocampal neurons resulted in an impaired retrograde trafficking of BACE1 and altered BACE1 distribution. Suppression of BACE1 expression rescued Vps35 deficiency induced deficits, suggesting a role of BACE1 in contributing to the Vps35 deficiency induced phenotypes during development. These results thus demonstrate a critical role for VPS35 in developing hippocampal neurons and yield insights into further mechanisms of retromer regulated AD pathogenesis in mature neurons.

Results

Shortened apical dendrites and swollen axons in Vps35 deficient CA1 neurons

To investigate possible functions of VPS35 in hippocampal neurons, we first examined VPS35's expression in developing and adult mouse hippocampus by taking advantage of the $Vps35^{+/m}$ mouse, in which the LacZ gene was "knocked-in" in the intron of the Vps35 gene, thus, LacZ expression is controlled by the promoter of the Vps35 gene (Wen et al., 2011). The β-gal activity was weakly and diffusely distributed in the hippocampal region of E15.5 mouse embryos, and became highly restricted to CA1–3 regions of the hippocampus in neonatal stage [e.g., postnatal day 10 (P10)] (Fig. 1A). The expression appeared to be peaked at the neonatal stage (P10–P15) of the hippocampus (Fig. 1A), and this view was also supported by the Western blot analysis (Fig. 1B). As P10–P15 is a critical time-window for the establishment of axonal–dendritic sorting, synaptogenesis, and circuitry of hippocampal neurons, the peak level of VPS35 expression at P10–P15 thus implicate VPS35 in these events.

We next examined VPS35's function in developing mouse CA1 neurons by use of the RNA interference (RNAi) technology and an *in utero* electroporation assay (supplementary material Fig. S1A–C). Several miRNA-Vps35 (miR-Vps35) constructs targeting different exons of Vps35 were generated, and miR-Vps35-1 and miR-Vps35-3 showed high and medial efficiency in knocking down Vps35 expression in HEK 293 cells, respectively, determined by Western blot assay (supplementary material Fig. S1D). The *in utero* electroporation of miR-Vps35-1 into the

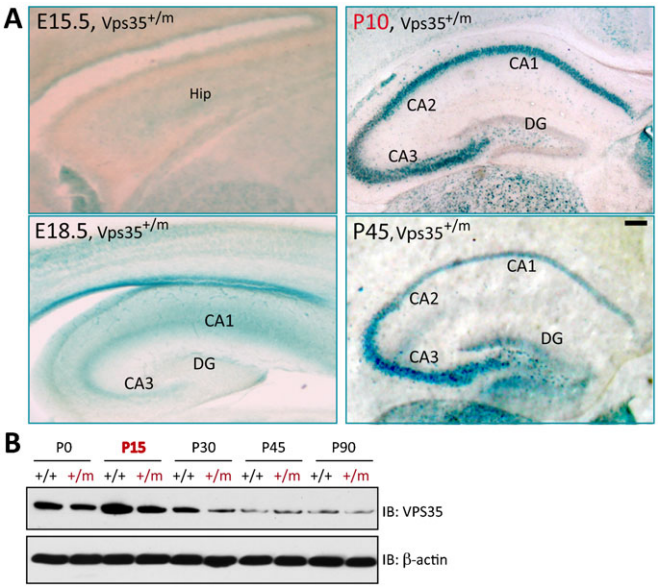

Fig. 1. Vps35 expression in developing mouse hippocampus. (**A**) Detection of enzymatic LacZ activity in developing $Vps35^{+/m}$ hippocampus. At the neonatal brain (e.g., P10–P15), LacZ activity detected in CA1–3 hippocampus was at its peak level. DG and CA1–3 in hippocampus are indicated. Scale bar: 200 µm. (**B**) Western blot analysis of VPS35 protein levels in lysates from $Vps35^{+/+}$ and $^{+/m}$ mouse hippocampus during development. Again, a highest level of VPS35 protein was detected in P15 hippocampus. Note that ~50% reduction of VPS35 protein was found in lysates from $Vps35^{+/m}$ mice, demonstrating the antibody specificity.

progenitor cells of CA1 pyramidal neurons in mouse hippocampus at E15.5 also markedly suppressed endogenous Vps35 expression (supplementary material Fig. S1E). At P10, the majority of miR-Vps35 transfected neurons had migrated to pyramidal cell layer of hippocampal CA1 region, however, a mild but significant migration defect was observed in miR-Vps35-1 neurons: ~13% of neurons were mislocated out of pyramidal cell layer as compared to ~5% in control (supplementary material Fig. S2). This migration defect was not observed in miR-Vps35-3 neurons (~5% mis-distribution), suggesting that the migration defect happens when VPS35 protein level was largely reduced. In addition, the apical dendrites of miR-Vps35-1 neurons were much shorter as compared to that of control neurons, which formed apical dendritic tufts in the superficial region of CA1 (Fig. 2A,B). The miR-Vps35-3 apical dendrites also displayed a similar but less severe phenotype as compared to that of miR-Vps35-1 (Fig. 2B,C), suggesting a Vps35 dose-dependency. The shortened apical dendrite phenotype developed initially at P7, a stage when control apical dendrites have not fully arborized (supplementary material Fig. S2). The loss of apical dendritic tufts in miR-Vps35-1 expressing CA1 neurons was not corrected at later stages of the development (e.g., P14 and P25) (Fig. 2C). Moreover, a reduced dendritic spine density with an increased spine head size was also observed in the Vps35 deficient CA1 neurons (Fig. 2D–F). These morphological dendritic defects suggest the importance of VPS35/retromer in promoting CA1 dendritic growth or maturation in developing CA1 neurons, and reveal a role for VPS35 in keeping healthy dendritic spine structure, which is critical for synapse formation and function.

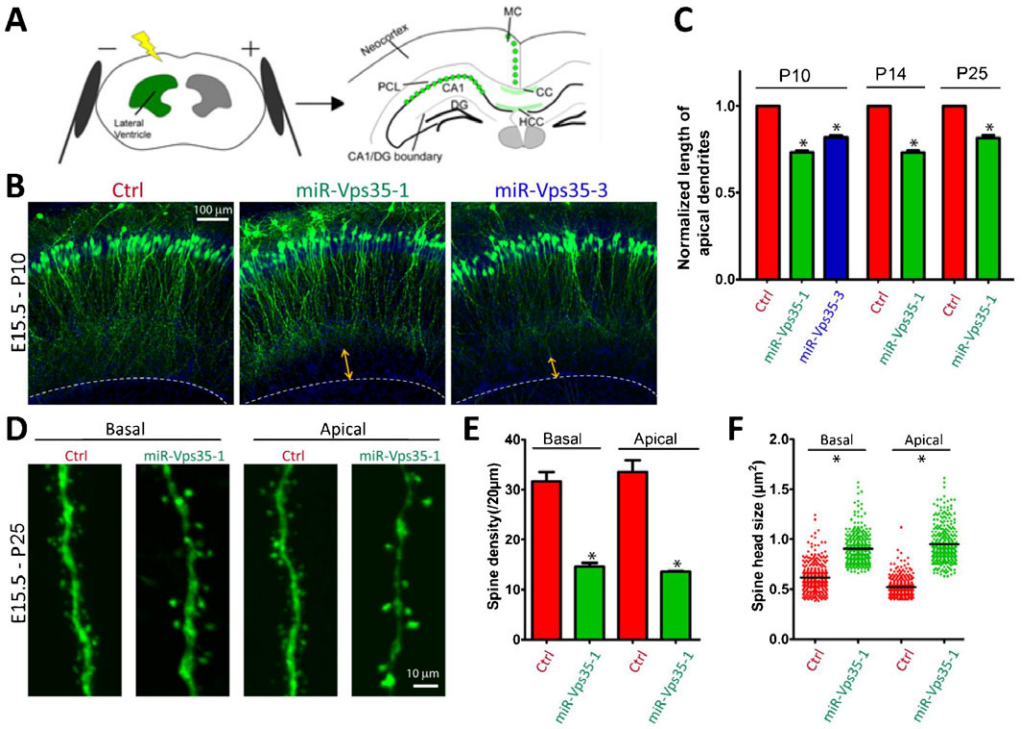

Fig. 2. Defective apical dendritic arborization and impaired spine morphology in Vps35 deficient mouse CA1 neurons. (**A**) Schematic illustration of the *in utero* electroporation experiments. Control and miRNA-Vps35 (miR-Vps35) constructs were *in utero* electroporated into E15.5 brains, and neurons and their dendrites in the hippocampal CA1 region were examined at P10, P14, or P25 postnatal stages. All images were counter-stained with Topro-3 (blue). (**B**) Shortened apical dendrites at P10 by miR-Vps35-1 and -3 electroporation compared to control dendrites. A blank area (yellow arrows) between the distal end of dendrites and pia surface (dotted line) was observed in Vps35-suppressed CA1 regions. Scale bar: 100 μm. (**C**) Quantification of apical dendritic lengths at different postnatal stages. *$P<0.01$, $n=3$–4 brains for each group. (**D**) Impaired spine morphology in basal and apical dendrites at P25 by miR-Vps35-1 electroporation compared to the control. Scale bar: 10 μm. (**E**,**F**) Quantification of spine density (E) and spine head size (F) in basal and apical dendrites. *$P<0.01$, $n=300$ spines from 3 different brains for each group.

We then asked if CA1 neuronal axonal outgrowth and morphology were affected by suppression of Vps35 expression. Hippocampal commissures (HCC), which contain most axons from CA1 neurons, were examined, and no significant defect was observed in viewing axonal length/outgrowth between the control and miR-Vps35 expressing neurons (data not shown). However, in comparing with the control miRNA expressing axons in the HCC, a marked increase of axonal swellings or spheroid formation (viewed by GFP with area size $> 10\ \mu m^2$) was observed in Vps35 deficient axons (Fig. 3A–C). The axonal

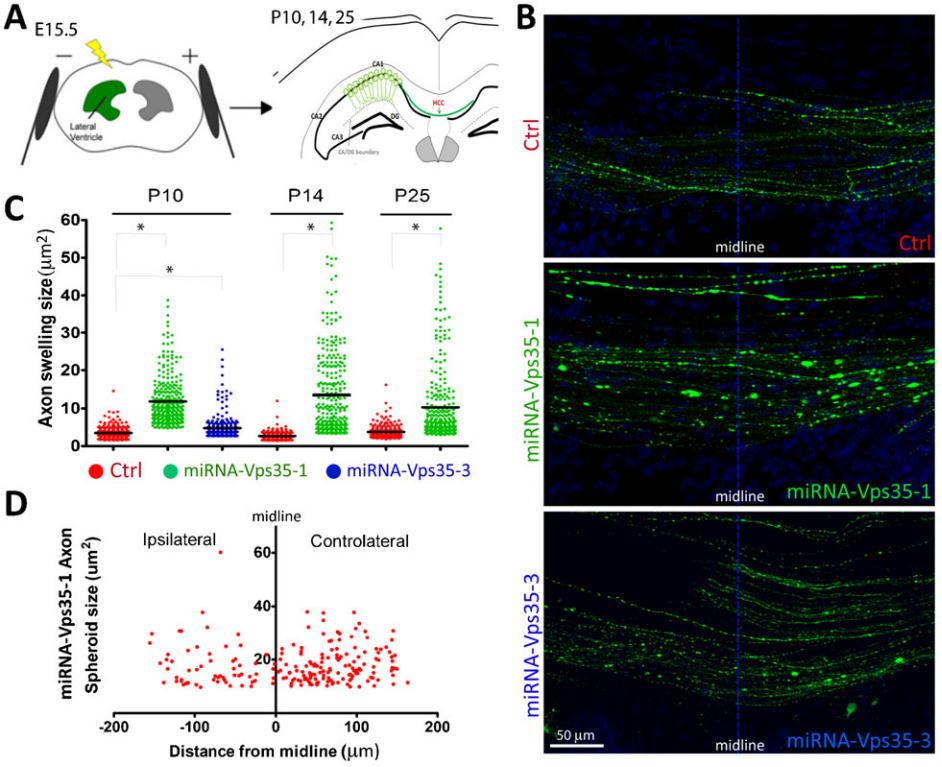

Fig. 3. Axonal spheroids in Vps35 deficient mouse CA1 neurons. (**A**) *In utero* electroporation of control, miR-Vps35-1 or -3 was performed at E15.5 and brains were examined at P10, P14, and P25. All images were counter-stained with Topro-3 (blue). Axonal morphology in HCC region was examined. (**B**) Representative images for increased axonal spheroids in HCC region at P10 by miR-Vps35-1 and -3. Dotted blue lines indicate the midline of the brain. Scale bar: 50 μm. (**C**) Quantification of axonal swelling size. *$P<0.01$, $n=300$ spheroids from 6 different brains for each group. (**D**) More severe spheroid formation on the contralateral side of HCC than that on the ipsilateral side. The spatial distribution pattern of axonal spheroids by miR-Vps35-1 electroporation was quantified and illustrated, and each dot represents a spheroid with size $> 10\ \mu m^2$. Data were from 6 brains at P10.

spheroid formation appeared to be more severe in the distal axons or in HCC after crossing midline as compared with that before crossing (Fig. 3D), and more obvious in miR-Vps35-1 expressing neurons as compared with that of miR-Vps35-3 (Fig. 3B,C). The axonal spheroid phenotype was not confined to HCC, but also present in callosal axons (CC) from cortical pyramidal neurons (data not shown).

Taken together, loss of VPS35 expression in hippocampal neurons caused apical dendrite growth defects, spine malformation, and swollen commissural axons, particularly in distal regions of dendrites and axons, during hippocampal development.

Defective retrograde trafficking of BACE1 in Vps35 deficient hippocampal neurons

The axonal swellings in Vps35 deficient neurons may reflect in a defective protein transport or trafficking. We thus examined if retromer cargos, including APP, SorLA, and BACE1, or subcellular organelles (early and late endosomes) were "trapped" in the spheroids due to Vps35 deficiency. Interestingly, APP and BACE1, but not SorLA, were identified in the spheroids (Fig. 4A,B,D). Also detected in the spheroids was the late endosome/early lysosome marker, LAMP1, but not early endosome marker, EEA1 (Fig. 4A,D). The absence of SorLA and EEA1 signals in the spheroids was not due to the inefficiency of the antibodies, as these antibodies recognized SorLA and EEA1 proteins as punctae patterns in CA1 soma and dendritic, particular basal dendritic compartments (Fig. 4B). Together, these results implicate that BACE1 and APP, possibly in the late endosomes, may require VPS35/retromer for their retrograde trafficking.

We further tested this view by examining BACE1's distribution and trafficking in Vps35 deficient neurons in culture and *in vivo* using BACE1-mCherry. BACE1-mCherry was predominantly distributed at the peri-nuclear vesicles, close to Golgi apparatus in the soma, and dendritic compartments of control neurons in culture (Fig. 5A–C). In contrast, the BACE1 punctae in Vps35 depleted neurons were enlarged in size, and no

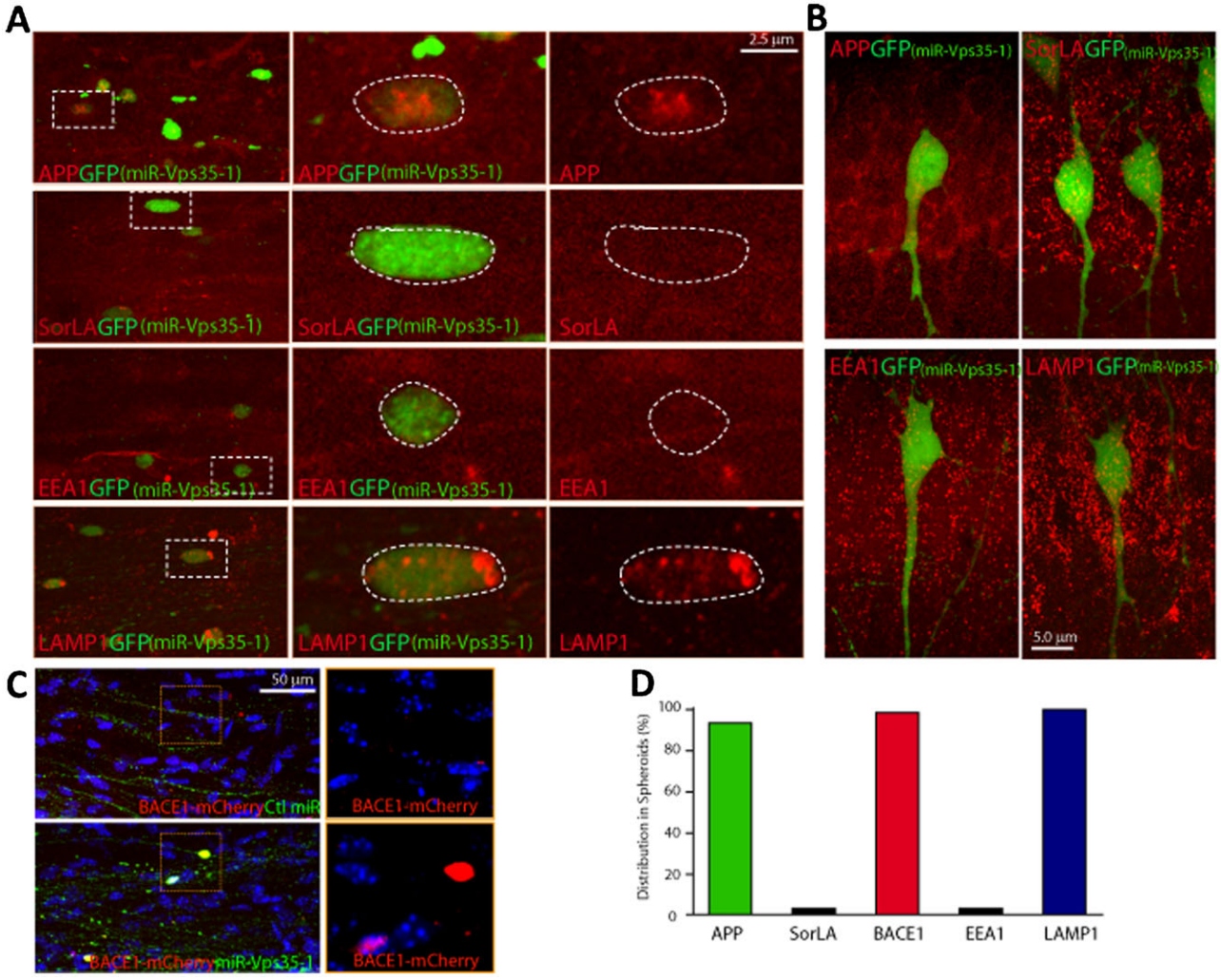

Fig. 4. Protein components in axonal spheroids induced by Vps35 deficiency. (**A**,**B**) *In utero* electroporation with miR-Vps35-1 was performed at E15.5 and brain slices at P14 were immunostained with different antibodies (APP, SORLA, EEA1 and LAMP1). Projected images from z-stack confocal scanning showing immunosignal (red) in HCC (A) and cell body (B) regions. Note that APP and LAMP1, but not SORLA and EEA1, appeared to be enriched in spheroids (A). Scale bar: 2.5 μm (A); 5.0 μm (B). (**C**) Co-electroporation of miR-Vps35-1 with BACE1-mCherry was performed at E15.5 and brain slices at P10 were scanned under confocal microscope. Note that BACE1-mCherry fusion proteins (red) were enriched in spheroids. Scale bar: 50 μm. (**D**) The percentages of spheroids enriched in indicated proteins were quantified. APP: 93.8%, $n=16$; SORLA: 0%, $n=18$; EEA1: 0%, $n=10$; LAMP1: 95.2%, $n=21$; BACE1-mCherry: 100%, $n=50$.

longer confined to the Golgi apparatus (Fig. 5A–C), suggesting the necessity of VPS35 in enriching BACE1 localization to the Golgi apparatus and proximal dendrites in neurons. Also observed was GFP "aggregates" or spheroid-like punctae in Vps35 deficient neurites (Fig. 5D,E). Further support for Vps35 regulating BACE1 trafficking *in vivo* was the observation of altered BACE1-mCherry distribution in Vps35 deficient mouse CA1 neurons by *in utero* electroporation (Fig. 6). It was largely distributed in the major apical dendrites of the control CA1 neurons, with peak level at the apical side of proximal dendrites, where Golgi or TGN is located (Fig. 6A,B) (data not shown). However, in CA1 neurons expressing miR-Vps35-1, BACE1-mCherry was distributed in both apical and basal dendrites without the enrichment at the proximal apical dendrites (Fig. 6B,C). Many BACE1-puncta were shifted to the basal side (Fig. 6C) and enlarged in size (Fig. 6D), in addition to be detected in the axonal spheroids in Vps35 deficient CA1 neurons (Fig. 6E). These results suggest that VPS35 may promote endosome-to-Golgi retrograde trafficking of BACE1 not only in primary rat hippocampal neurons, but also in mouse CA1 neurons, not only in dendrites, but also in axons.

To further test if BACE1's retrograde trafficking is affected in Vps35 deficient neurons, we viewed BACE1-mCherry's movement in control and Vps35 depleted neurons by time-lapse imaging analysis. BACE1-mCherry labeled vesicles exhibited both active anterograde and retrograde movement along neurites in the control neurons (Fig. 7A–D). In contrast, Vps35 depletion resulted in a defective retrograde movement of BACE1-mCherry towards the soma, without obvious effect on its anterograde movement (Fig. 7A–D). Consequently, the ratio of BACE1-mCherry vesicle in the stationary phase was increased in the Vps35 deficient neurons (Fig. 7E). These results thus demonstrate that Vps35 depletion impaired retrograde trafficking/transport of BACE1 in neurons.

Rescue of Vps35 deficiency induced dendritic and axonal deficits in CA1 neurons suppressing BACE-1 expression

We next asked if BACE1 contributes to Vps35 deficiency induced CA1 neuropathology. To this end, we examined whether suppressing BACE1 can rescue Vps35 deficiency induced dendritic and/or axonal phenotypes. The plasmids encoding miRNA-Bace1 (miR-Bace1) were generated, and the miR-Bace1-1 suppressed BACE1 expression specifically and efficiently (supplementary material Fig. S3A). This plasmid was thus co-electroporated with miR-Vps35-1 in mouse embryos (E15.5), and their apical dendrites and axons at P10 were evaluated in comparison with that expressing miR-Vps35-1 with the control (Fig. 8A). Remarkably, both distal dendritic loss and axonal spheroid formation were greatly rescued when miR-Bace1-1 was co-expressed (Fig. 8A–C). This rescue effect was

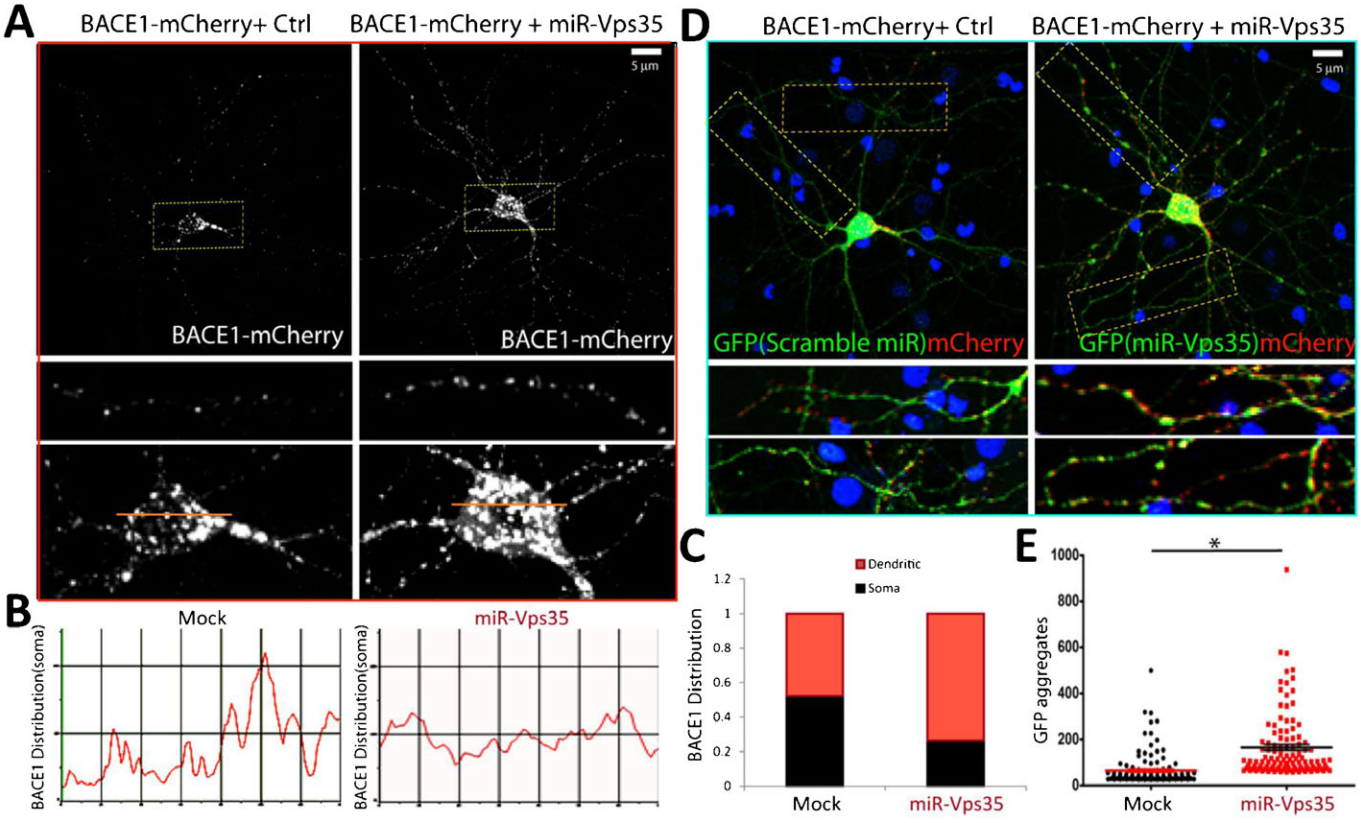

Fig. 5. Altered BACE1 distribution in primary hippocampal neurons expressing miR-Vps35-1. Co-transfection of BACE1-mCherry with control or miR-Vps35-1 was performed in primary rat hippocampal neurons (E18) at DIV 5. Confocal imaging analysis of transfected neurons at DIV 9 was carried out and representative images were shown (**A**,**D**). Scale bar: 5 μm. The middle and lower panels showed the amplified images of the boxed areas. (**B**) Quantification analysis of the density of BACE1-mCherry fluorescence crossing the lines indicated in lower panels of A. (**C**) Quantification analysis of the percentage of BACE1-mCherry puncta in soma (black column) *vs* dendrite (orange column) regions. (**E**) Quantification analysis of the size of GFP-aggregates from D. The sizes of the top 100 GFP aggregates were showed as the grouped column scatter. The line in the scatter indicated the median. *, $P<0.05$.

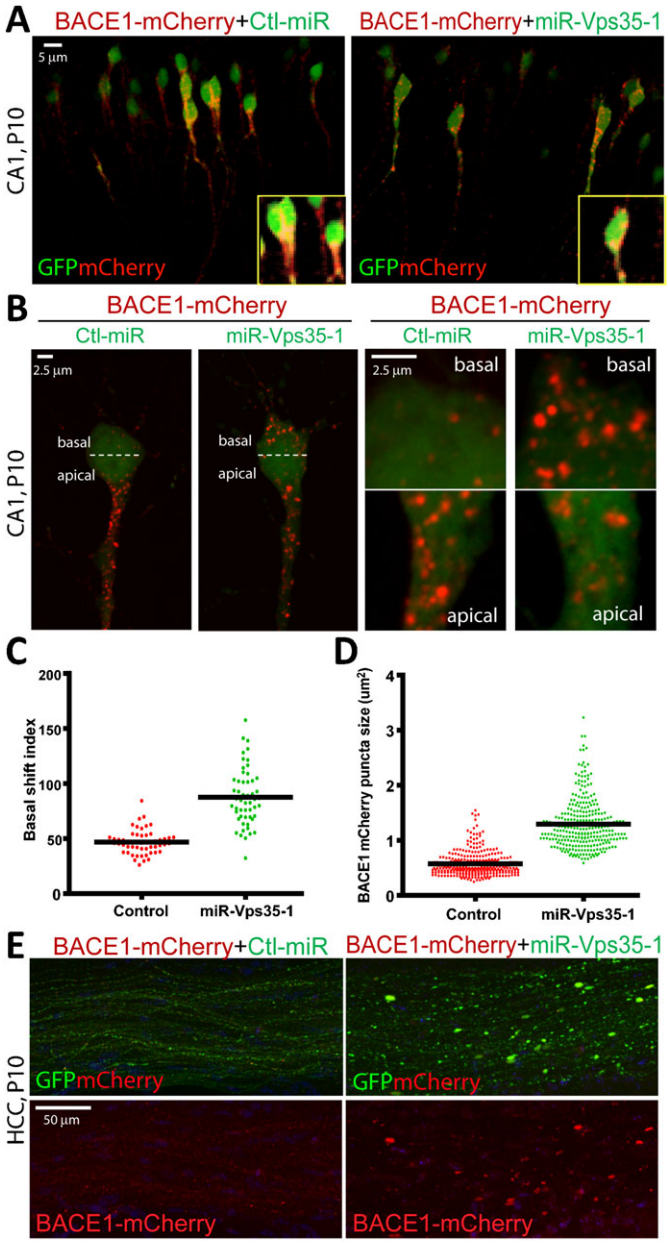

Fig. 6. Altered BACE1 distribution in Vps35 deficient mouse CA1 neurons. Co-electroporation of BACE1-mCherry with control miRNA or miR-Vps35-1 was performed at E15.5 embryos *in utero* and brain slices were examined at P10. (**A**) Representative images showing BACE1-mCherry distribution in the proximal apical dendrites of the CA1 neurons. Inserts of enlarged images showing basal shift of BACE-mCherry signal in VPS35 deficient neurons. Scale bar: 5 μm. (**B**) Sample images at higher magnification showing BACE1-mCherry aggregation and basally shifted redistribution. Scale bar: 2.5 μm. (**C**) Quantification analysis of BACE1-mCherry distribution in miR-VPS35-1 neurons and control neurons. Basal shift index (BSI; see Materials and Methods) was introduced to judge the degree of BACE-mCherry redistribution from apical to basal side of the neuron. Bars showing average BSI (Control: 46.8; miR-VPS35-1: 87.5; $n=54$ from 3 brains for each group). (**D**) Quantification analysis of BACE1-mCherry aggregation in miR-VPS35-1 neurons and control neurons. The size of BACE1-mCherry puncta was measured (see Materials and Methods) ($n=300$ from 3 brains for each group). The bars showing average size of BACE1-mCherry puncta (Control: 0.57 μm^2; miR-VPS35-1: 1.29 μm^2). (**E**) Representative images of BACE1-mCherry distribution in control and Vps35 deficient CA1 axons in HCC region. Scale bar: 50 μm.

not due to the inhibition of miR-Vps35-1's suppressing activity on Vps35 expression, as Vps35's expression in CA1 neurons was also markedly reduced by both electroporations (miR-Vps35+control *vs* miR-Vps35-1+miR-Bace1) (supplementary material Fig. S3B). These results suggest that the morphological changes in Vps35 deficient CA1 neurons are BACE1-dependent.

Discussion

In this paper, we showed that loss of Vps35 expression in developing mouse hippocampal neurons results in developmental defects, including shorter apical dendrites, reduced dendritic spines, and increased swollen axons. We further showed that BACE1, a critical cargo of retromer in CA1 neurons, contributes to Vps35 deficiency induced CA1 neuropathology during development. These observations thus establish an important role for VPS35 in promoting retrograde transport of BACE1 in developing hippocampal neurons, leading to a working model depicted in Fig. 8D, and providing insights into the pathogenesis of neurodegenerative disorders in adults.

Using *in utero* electroporation of miRNA to suppress Vps35 expression in embryonic CA1 neurons in a wild type background, we are able to assess the cell autonomous function of Vps35/retromer during mouse hippocampal development. The morphological phenotypes due to Vps35 depletion in developing CA1 neurons suggest a dependence of VPS35/retromer in hippocampal neuron morphogenesis *in vivo*. In carefully examining the phenotypes, it was revealed that the loss of apical dendritic tuft was restricted to the distal, but not proximal, regions of Vps35 deficient CA1 neurons, and the axonal swollen were more severe in HCC after midline crossing (Fig. 3D). These observations thus suggest that VPS35/retromer may have a more important role in the distal regions of dendrites and axons, implicating a neuronal regional dependence of VPS35. The regional dependence between proximal and distal dendrites of CA1 neurons is also reported in adult rat hippocampal slices, in which L-LTD (longer-lasting forms of long term depression) is induced in the distal, but not proximal, apical dendrites of CA1 neurons (Parvez et al., 2010). In addition, the cytoplasmic dynein heavy chain 1, a motor moving toward the minus ends of microtubules, also functions in a regional dependent manner (Hirokawa et al., 2010). It is essential for retrograde transport of cargos in distal dendrites and axons, but not in proximal dendrites, where dynein conveys cargos to both the periphery and soma regions (Hirokawa et al., 2010) (Fig. 8D). This regional dependent dynein-mediated transport is believed due to the mixed polarity of the microtubules in the proximal dendrites, but highly polarized microtubules in the distal dendrites and axons (Conde and Cáceres, 2009; Hirokawa et al., 2010). In light of these observations, we speculate that the regional dependent phenotypes in Vps35 deficient CA1 neurons may reflect in its function in promoting dynein mediated retrograde transport of cargos (Fig. 8D). Further support for this view are observations that SNX5/6, a subcomponent of retromer, interacts with not only BACE1 (Okada et al., 2010), but also $p150^{Glued}$ component of dynactin, an activator of dynein motor complex (Hong et al., 2009; Wassmer et al., 2009), and that impaired retrograde, but not anterograde, movement of BACE1 was observed in Vps35 deficient neurons (Fig. 7). These results thus reveal a molecular link underlying VPS35/retromer regulating dynein mediated retrograde transport (Fig. 8D).

BACE1, an essential membrane proteinase for APP metabolism, is involved in AD pathogenesis (Vassar and Kandalepas, 2011). It is believed to be a cargo of retromer based on cell culture studies

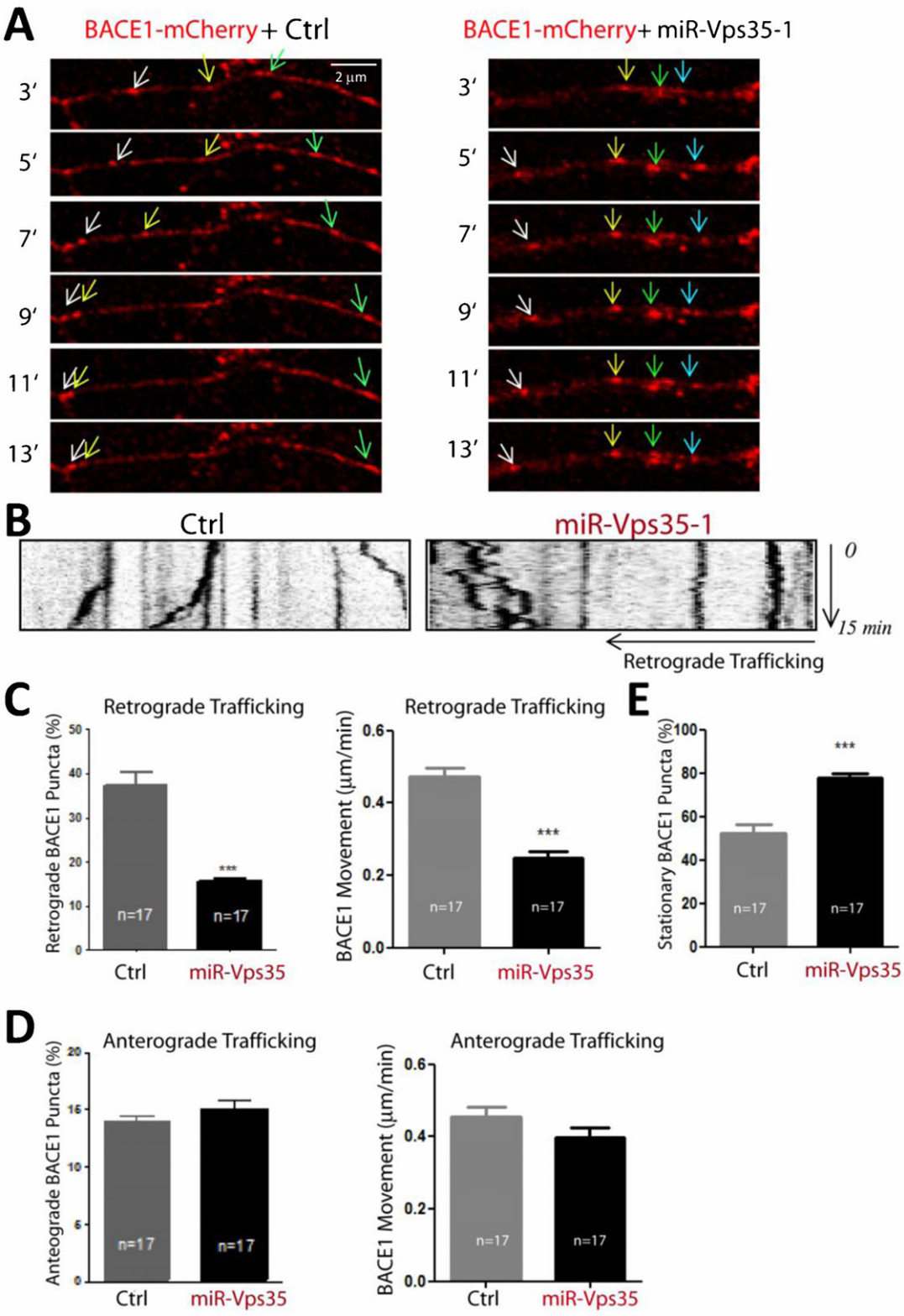

Fig. 7. Defective BACE1-mCherry retrograde trafficking in primary hippocampal neurons expressing miR-Vps35-1. (**A**) Representative images showing distribution patterns of BACE1-labeled vesicles in control and miR-Vps35-1 expressing hippocampal neurons. Neurons were co-transfected with BACE1-mCherry with control and miR-Vps35-1 at DIV5 and followed by time-lapse imaging analysis 48 hours after transfection. Scale bar: 2 µm. (**B**) Representative kymographs showing the mobility of BACE1 positive vesicles/endosomes during 15-min recordings in control and miR-Vps35 expressing neurons. Vertical lines represent stationary BACE1-vesicles; oblique lines or curves to the right represent anterograde movements and lines to the left indicate retrograde transport. (**C–E**) Relative mobility (anterograde, retrograde, and stationary) of BACE1-vesicles in control and miR-Vps35-1 expressing neurons. Data were quantified from the total number of 17 BACE1-vesicles in neurons from >3 experiments, as indicated in parentheses. Error bars: S.D. *P<0.01.

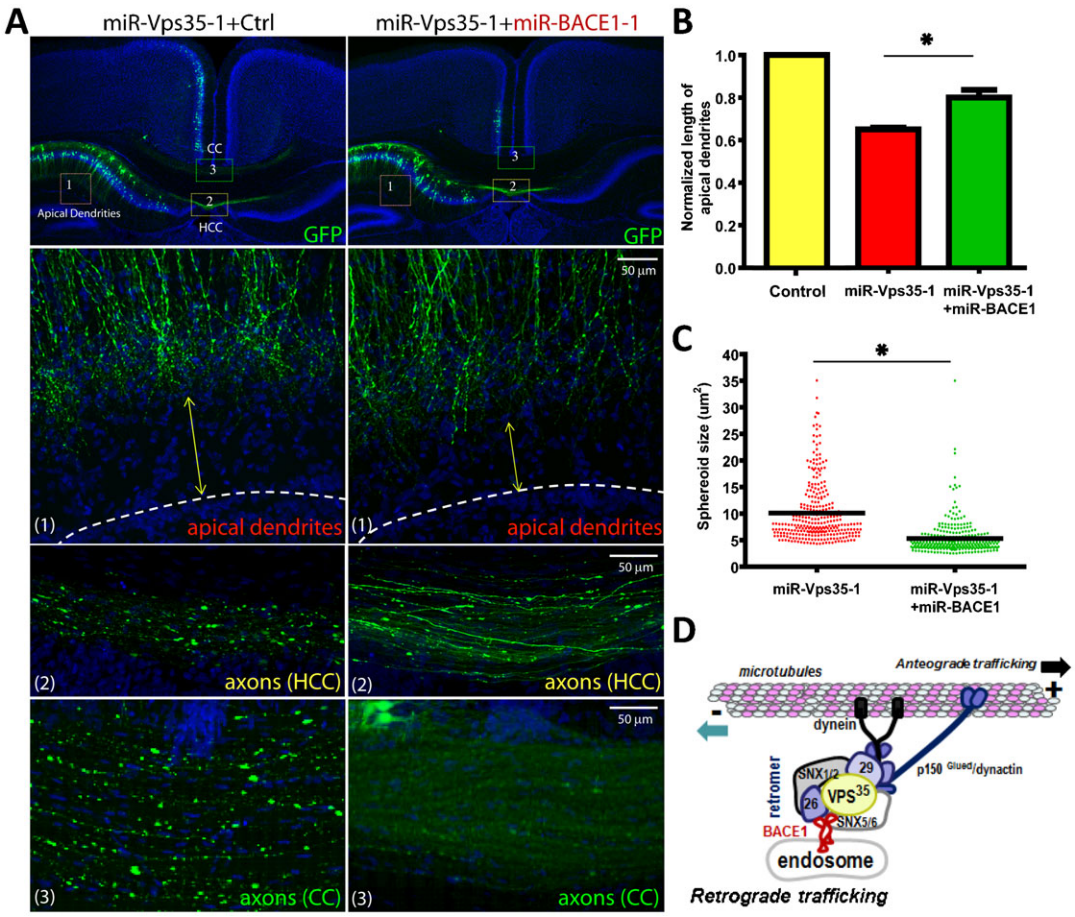

Fig. 8. Rescue of Vps35 deficiency induced axonal spheroids and apical dendritic arborization defect by suppressing BACE1 expression. Co-electroporation of miR-VPS35-1 with control construct or miR-BACE1 was performed at E15.5 *in utero* and brains were examined at P10. (**A**) Effects of miR-BACE1 on miR-VPS35 induced axon- and dendrite-defects. Upper panels, similar distribution pattern and cell density of electroporated cells between miR-VPS35-1+control and miR-VPS35-1+miR-BACE1 shown in low magnification. Middle panels, apical dendrites in the distal region were much longer in miR-VPS35-1+miR-BACE1 than in miR-VPS35-1+control. Lower panels, spheroids in miR-VPS35-1+miR-BACE1 expressing axons in HCC and CC regions were greatly reduced compared to that in miR-VPS35-1+control. Scale bar: 50 μm. (**B**) Quantification of apical dendrite growth by measuring normalized length of apical dendrites. miR-VPS35-1+miR-BACE1 expression dendrites were significantly longer than control miR-VPS35-1 dendrites (*$P<0.01$). (**C**) Quantification of axon spheroid formation by measuring the size of swellings in commissural axons ($n=300$ from 3 brains for each group). Bars showing average size of selected swellings (miR-VPS35-1+control: 9.16 μm^2; miR-VPS35-1+miR-BACE1: 5.36 μm^2). The percentage of spheroids (>10 μm^2) is 29% for miR-VPS35-1+control and 5% for miR-VPS35-1+miR-BACE1. (**D**) Schematic illustration of a working model for VPS35 containing retromer in promoting retrograde transport of BACE1.

(Okada et al., 2010; Finan et al., 2011). Our current work supports this notion and provides further evidence for BACE1 as a cargo of retromer not only in neuronal culture but also in mouse. Our studies also suggest that the BACE1 contributes to the Vps35 deficiency induced phenotypes, as suppressing BACE1 expression in CA1 neurons rescued the phenotypes (Fig. 8), revealing the importance to control BACE1 trafficking and distribution by retromer.

In addition to a defective retrograde trafficking of BACE1, Vps35 depletion in CA1 neurons also results in a loss of dendritic spine. Dendritic spines are small actin-rich protrusions that form the postsynaptic part of most excitatory synapses (Hoogenraad and Akhmanova, 2010). They are highly dynamic structures and play crucial roles in synaptic functions during learning and memory (Hoogenraad and Akhmanova, 2010; Svitkina et al., 2010). It is unclear how VPS35 regulates dendritic spine dynamics. The decreased dendritic spines may be due to a defective membrane protein trafficking and/or actin remodeling in Vps35 deficient CA1 neurons. In fact, retromer/VPS35 is implicated in actin remodeling as it interacts with WASH protein complex (Seaman, 2007; Gomez and Billadeau, 2009; Harbour et al., 2012), an important complex for actin remodeling, receptor endocytosis, and tubulin cross talk. Thus, it is conceivable that loss of Vps35 function may results in an impaired WASH1 mediated actin remodeling in dendrites, leading to a reduction in dendritic spine density but increase in the spine head size. However, this speculation requires further investigation.

It is worth noting that VPS35 deficiency induced dendritic and axonal phenotypes in developing brain resemble to the morphological changes observed in neurodegenerative diseases in adult. However, we did not observe obvious neuronal loss even at 6-month-old Vps35$^{+/m}$ mice (data not shown), suggesting that ~50% reduction in VPS35 expression alone in neurons does not result in neurodegeneration in young animals. Due to the limitation of our *in vivo* knock-down approach, which does not allow longer term (e.g., > 40 days after electroporation) expression of the miRNAs, we are unable to address whether VPS35 deficiency causes neuronal degeneration in older mice.

This will again need more systematic studies by employing strategies such as conditional knock-out of Vps35. Nevertheless, the molecular mechanisms for VPS35 deficiency induced deficits in developing hippocampus may facilitate the pathogenic dissection of mechanisms underlying Vps35-loss associated neurodegeneration in mature neurons.

In summary, the data presented in this manuscript suggest an important function of VPS35 in dendritic growth or maturation and in preventing axonal spheroid formation during mouse hippocampal development. These functions may be due to retromer regulation of dynactin/dynein mediated retrograde transport of membrane proteins, such as BACE1. It remains an open question whether the early developmental defects induced by VPS35 deficiency may partially contribute to the evolvement of neurodegeneration by VPS35 mutation observed in human genetic diseases including AD and PD.

Materials and Methods

Reagents and animals

Rabbit polyclonal anti-VPS35 antibody was generated using the antigen of GST–VPS35D1 fusion protein as described (Small et al., 2005b; Wen et al., 2011).

Vps35 mutant mice were generated by injection of mutant embryonic stem (ES) cells obtained from Bay Genomics as described previously (Wen et al., 2011). The wild type pregnant mice in CD1 background were used for *in utero* electroporation. All experimental procedures were approved by the Animal Subjects Committee at the Georgia Health Sciences University, according to US National Institutes of Health guidelines.

Expression plasmids

The miRNA-Vps35 or miRNA-BACE1 expression vectors were initially generated by the BLOCK-iT Pol II miR RNAi expression System (Invitrogen, Carlsbad, CA) according to the manufacturer's instruction (Wen et al., 2011). Oligonucleotide sequences for miRNA constructs were below.

miR-VPS35-1:

5′ TGCTGTAACGTTCCACATTTACACCTGTTTTGGCCACTGACTGACAGGTGTAAGTGGAACGTTA3′ (sense);

5′ CCTGTAACGTTCCACTTACACCTGTCAGTCAGTGGCCAAAACAGGTGTAAATGTGGAACGTTAC3′ (antisense);

Targeting sequence: AGGTGTAAATGTGGAACGTTA

miR-VPS35-3:

5′ TGCTGTAATTCAGCCAGCTCAGCTTTGTTTTGGCCACTGACTGACAAAGCTGATGGCTGAATTA3′ (sense);

5′ CCTGTAATTCAGCCATCAGCTTTGTCAGTCAGTGGCCAAAACAAAGTGAGCTGGCTGAATTAC3′ (antisense);

Targeting sequence: AAAGCTGAGCTGGCTGAATTA

miR-BACE1:

5′ TGCTGAATGTTGGCACGCACAGTGACGTTTTGGCCACTGACTGACGCACTGTGTGCCAACATT3′ (sense);

5′ CCTGAATGTTGGCACACAGTGACGTCAGTCAGTGGCCAAAACGTCACTGTGCGTGCCAACATTC3′ (antisense);

Targeting sequence: GTCACTGTGCGTGCCAACATT

The miRNA sequence fragments were initially subcloned into pcDNA^{TM} 6.2-GW/EmGFP-miR vector. To allow miRNA plasmids suitable for *in vivo* expression, the miRNA sequence fragments in pcDNA^{TM}6.2-GW/EmGFP-miR vector were released by SalI and XhoI restriction digestion and subcloned into CAG-IRES-EGFP expression plasmid at the XhoI site. Their suppressing effects were verified by Western blot analysis of lysates co-expressing miRNA plasmids with Vps35 or BACE1 expressing plasmids.

The cDNAs encoding full length Vps35 was amplified by PCR and sub-cloned into mammalian expression vectors downstream of a signal peptide and a Flag epitope tag (MDYKDDDDKGP) and under control of the CMV promoter as described previously (Ren et al., 2004; Xie et al., 2005; Wen et al., 2011). The plasmid encoding BACE1-mCherry was generated by fusion of the mCherry to the C-terminus of the RT-PCR amplified mouse BACE1 in a mammalian expression vector under control of the CAG promoter. The plasmid of BACE1-HA was kindly provided by Dr R.Q. Yan (Cleveland Clinic) (He et al., 2004). The authenticity of all constructs was verified by DNA sequencing and Western blot analysis.

β-Gal detection

Whole amount Vps35$^{+/m}$ embryos at different stage of development or brain sections derived from various stages of Vps35$^{+/m}$ embryos were fixed with 0.5% glutaraldehyde and incubated with X-gal solution (2 mM MgCl2, 5 mM potassium ferricyanide, and 0.1% X-gal) in dark at 37℃ for 8 hours as described previously (Lee et al., 2010; Zhou et al., 2010; Wen et al., 2011).

In utero electroporation

The *in utero* electroporation was carried out as described previously with some modifications (Wang et al., 2007). Briefly, pregnant mice at E15.5 anesthetized and maintained through isoflurane inhalation were subjected to abdominal incision to expose the uterus. Through the uterine wall, embryos were visualized, and plasmids (1.5 μg/μl for each) were injected into the lateral ventricle through a glass capillary. Embryos will then subjected to electroporation (ten 50-ms, 33v pulses at an interval of 1 s) through ECM-830 (BTX, Holliston, MA). Uterine horns were repositioned into the abdominal cavity before the abdominal wall and the skin were sutured. Pups were reared to different postnatal stages. Under deep anesthesia, mice were perfused transcardially with 0.1 m phosphate buffer (PBS) followed by 4% paraformaldehyde in PBS, pH 7.4. At each time-point, at least six pups (three for each construct mix) were used for data analysis in each set of experiments. The brains of the pups were overnight-fixed and cut into floating slices at different thickness according to the age (80 μm for P10, 100 μm for P14 and 120 μm for $P>21$) using Leica vibratome cutting system. The slices were subjected to the confocal imaging analyses.

Immunofluorescence staining and confocal imaging analysis

For immunofluorescence staining of brain slices, age-matched electroporated littermates were perfused transcardially with 4% paraformaldehyde in PBS and brain tissues were post-fixed at 4℃ for 24 hours. Floating slices (50 μm in thickness) were incubated with indicated 1st and 2nd antibodies as described previously (Wen et al., 2011). The immunostained slices were then incubated with the PBS for an hour before imaging. For immunofluorescence staining analysis of transfected neurons, primary cultured neurons on the coverslips were fixed with 4% paraformaldehyde and 4% sucrose at room temperature for 45 min, permeabilized in 0.15% Triton X-100 for 8 min, and then subjected to co-immunostaining analysis using indicated antibodies as described previously (Zhu et al., 2007). Confocal images were obtained using Nikon C1 confocal system (for brain slices) or Zeiss LSM 510 (for culture neurons).

Image acquisition and data analysis

All the measurements on the brain sections were performed at the approximate level of bregma −2.18. For analysis of apical dendritic length of CA1 pyramidal neurons, the total area of EGFP labeled apical dendrites from the exit point of pyramidal cell layer to the distal end of apical dendrites were measured and normalized to the total area from the exit point of pyramidal cell layer to the pia surface (the boundary between CA1 and dentate gyrus). One normalized value of apical dendrite length was obtained from one brain and a total of 3–4 brains were measured for each group. For analysis of spine morphology, a total of about 2 mm dendrites from 3 brains for each group were examined. Spine density was calculated as the average number on a 20 μm length scale. For analysis of spine size, 100 largest spines from each section (one section from one brain) were identified and their head sizes were measured. 300 values of each group were pooled together for comparison between groups. For analysis of axonal spheroid formation in commissural axons, the sizes of 100 largest swellings from each section (one section from one brain) were measured and a total of 3 brains were examined for each group. 300 values of each group were pooled together for comparison between groups. For analysis of distribution pattern of axonal spheroids, the sizes of axonal swellings (>10 μm^2) and their distances relative to the brain midline were measured and a total of 6 brains electroporated with miVPS35-1 were examined. The size and distance of each spheroid was plotted. For analysis of BACE1-mCherry puncta size, 5 neurons from one brain were randomly chosen and 20 largest punctae from each neuron were measured for their sizes. A total of 300 punctae from each group ($n=3$) were pooled together for comparison between groups. For analysis of BACE-mCherry distribution, the ratio of BACE1-mCherry intensity on the basal side to that on the apical side was calculated and the ratio×100 was defined as a basal shift index. The values in each group ($n=54$ from 3 animals) were pooled together for comparison between groups.

Cell culture, transient transfection, and kymographs

HEK293 cells were maintained in Dulbecco modified Eagle medium supplemented with 10% fetal calf serum, and 100 units/mL of penicillin G and streptomycin (Gibco). Primary rat E18 hippocampal neurons were cultured as previously described (Zhu et al., 2007). Calcium phosphate method was used for transfection of HEK293 cells. Forty-eight hours following transfection, cells were lysed in modified RIPA immunoprecipitation assay buffer (50 mM Tris-HCl, pH 7.4, 150 mM sodium chloride, 1% NP40, 0.25% sodium-deoxycholate, proteinase inhibitors). Lysates and medium were subjected to immunoblotting analyses. Neurons were transfected with various constructs at DIV3 using the calcium phosphate method followed by immunocytochemistry or time-lapse imaging analysis 48 hours after transfection as described previously (Zhu et al.,

2007; Liu et al., 2012). Kymographs were made using extra plugins for ImageJ (NIH). The height of the kymographs represents recording time (15 min), and the width represents the length (in mm) of the neurite imaged.

Statistical analysis

Images are representative from at least three repeats. All data were expressed as mean ± SD. All data were analyzed by Student's T-test. The significance level was set at $P<0.05$.

Acknowledgements

We thank Drs Tae-Wan Kim and Riqiang Yan for reagents, and members of the Xiong and Mei laboratories for helpful discussions. This study was supported in part by grants from NINDS, National Institutes of Health (W.C.X. and L.M.), and grant from VA.

Competing Interests

The authors have no competing interests to declare.

References

Arighi, C. N., Hartnell, L. M., Aguilar, R. C., Haft, C. R. and Bonifacino, J. S. (2004). Role of the mammalian retromer in sorting of the cation-independent mannose 6-phosphate receptor. *J. Cell Biol.* **165**, 123-133.

Belenkaya, T. Y., Wu, Y., Tang, X., Zhou, B., Cheng, L., Sharma, Y. V., Yan, D., Selva, E. M. and Lin, X. (2008). The retromer complex influences Wnt secretion by recycling wntless from endosomes to the trans-Golgi network. *Dev. Cell* **14**, 120-131.

Bonifacino, J. S. and Hurley, J. H. (2008). Retromer. *Curr. Opin. Cell Biol.* **20**, 427-436.

Canuel, M., Lefrancois, S., Zeng, J. and Morales, C. R. (2008). AP-1 and retromer play opposite roles in the trafficking of sortilin between the Golgi apparatus and the lysosomes. *Biochem. Biophys. Res. Commun.* **366**, 724-730.

Chen, D., Xiao, H., Zhang, K., Wang, B., Gao, Z., Jian, Y., Qi, X., Sun, J., Miao, L. and Yang, C. (2010). Retromer is required for apoptotic cell clearance by phagocytic receptor recycling. *Science* **327**, 1261-1264.

Conde, C. and Cáceres, A. (2009). Microtubule assembly, organization and dynamics in axons and dendrites. *Nat. Rev. Neurosci.* **10**, 319-332.

Eaton, S. (2008). Retromer retrieves wntless. *Dev. Cell* **14**, 4-6.

Feinstein, T. N., Wehbi, V. L., Ardura, J. A., Wheeler, D. S., Ferrandon, S., Gardella, T. J. and Vilardaga, J. P. (2011). Retromer terminates the generation of cAMP by internalized PTH receptors. *Nat. Chem. Biol.* **7**, 278-284.

Finan, G. M., Okada, H. and Kim, T. W. (2011). BACE1 retrograde trafficking is uniquely regulated by the cytoplasmic domain of sortilin. *J. Biol. Chem.* **286**, 12602-12616.

Franch-Marro, X., Wendler, F., Guidato, S., Griffith, J., Baena-Lopez, A., Itasaki, N., Maurice, M. M. and Vincent, J. P. (2008). Wingless secretion requires endosome-to-Golgi retrieval of Wntless/Evi/Sprinter by the retromer complex. *Nat. Cell Biol.* **10**, 170-177.

Gomez, T. S. and Billadeau, D. D. (2009). A FAM21-containing WASH complex regulates retromer-dependent sorting. *Dev. Cell* **17**, 699-711.

Harbour, M. E., Breusegem, S. Y. and Seaman, M. N. (2012). Recruitment of the endosomal WASH complex is mediated by the extended 'tail' of Fam21 binding to the retromer protein Vps35. *Biochem. J.* **442**, 209-220.

He, W., Lu, Y., Qahwash, I., Hu, X. Y., Chang, A. and Yan, R. (2004). Reticulon family members modulate BACE1 activity and amyloid-β peptide generation. *Nat. Med.* **10**, 959-965.

Hirokawa, N., Niwa, S. and Tanaka, Y. (2010). Molecular motors in neurons: transport mechanisms and roles in brain function, development, and disease. *Neuron* **68**, 610-638.

Hong, Z., Yang, Y., Zhang, C., Niu, Y., Li, K., Zhao, X. and Liu, J. J. (2009). The retromer component SNX6 interacts with dynactin p150(Glued) and mediates endosome-to-TGN transport. *Cell Res.* **19**, 1334-1349.

Hoogenraad, C. C. and Akhmanova, A. (2010). Dendritic spine plasticity: new regulatory roles of dynamic microtubules. *Neuroscientist* **16**, 650-661.

Iwaki, T., Hosomi, A., Tokudomi, S., Kusunoki, Y., Fujita, Y., Giga-Hama, Y., Tanaka, N. and Takegawa, K. (2006). Vacuolar protein sorting receptor in *Schizosaccharomyces pombe*. *Microbiology* **152**, 1523-1532.

Kim, E., Lee, Y., Lee, H. J., Kim, J. S., Song, B. S., Huh, J. W., Lee, S. R., Kim, S. U., Kim, S. H., Hong, Y. et al. (2010). Implication of mouse Vps26b-Vps29-Vps35 retromer complex in sortilin trafficking. *Biochem. Biophys. Res. Commun.* **403**, 167-171.

Lee, D.-H., Zhou, L.-J., Zhou, Z., Xie, J.-X., Jung, J.-U., Liu, Y., Xi, C.-X., Mei, L. and Xiong, W.-C. (2010). Neogenin inhibits HJV secretion and regulates BMP-induced hepcidin expression and iron homeostasis. *Blood* **115**, 3136-3145.

Liu, Y., Peng, Y., Dai, P. G., Du, Q. S., Mei, L. and Xiong, W. C. (2012). Differential regulation of myosin X movements by its cargos, DCC and neogenin. *J. Cell Sci.* **125**, 751-762.

McGough, I. J. and Cullen, P. J. (2011). Recent advances in retromer biology. *Traffic* **12**, 963-971.

Muhammad, A., Flores, I., Zhang, H., Yu, R., Staniszewski, A., Planel, E., Herman, M., Ho, L., Kreber, R., Honig, L. S. et al. (2008). Retromer deficiency observed in Alzheimer's disease causes hippocampal dysfunction, neurodegeneration, and Aβ accumulation. *Proc. Natl. Acad. Sci. USA* **105**, 7327-7332.

Okada, H., Zhang, W., Peterhoff, C., Hwang, J. C., Nixon, R. A., Ryu, S. H. and Kim, T. W. (2010). Proteomic identification of sorting nexin 6 as a negative regulator of BACE1-mediated APP processing. *FASEB J.* **24**, 2783-2794.

Pan, C. L., Baum, P. D., Gu, M., Jorgensen, E. M., Clark, S. G. and Garriga, G. (2008). *C. elegans* AP-2 and retromer control Wnt signaling by regulating mig-14/Wntless. *Dev. Cell* **14**, 132-139.

Parvez, S., Ramachandran, B. and Frey, J. U. (2010). Functional differences between and across different regions of the apical branch of hippocampal CA1 dendrites with respect to long-term depression induction and synaptic cross-tagging. *J. Neurosci.* **30**, 5118-5123.

Port, F., Kuster, M., Herr, P., Furger, E., Bänziger, C., Hausmann, G. and Basler, K. (2008). Wingless secretion promotes and requires retromer-dependent cycling of Wntless. *Nat. Cell Biol.* **10**, 178-185.

Ren, X. R., Ming, G. L., Xie, Y., Hong, Y., Sun, D. M., Zhao, Z. Q., Feng, Z., Wang, Q., Shim, S., Chen, Z. F. et al. (2004). Focal adhesion kinase in netrin-1 signaling. *Nat. Neurosci.* **7**, 1204-1212.

Rogaeva, E., Meng, Y., Lee, J. H., Gu, Y., Kawarai, T., Zou, F., Katayama, T., Baldwin, C. T., Cheng, R., Hasegawa, H. et al. (2007). The neuronal sortilin-related receptor SORL1 is genetically associated with Alzheimer disease. *Nat. Genet.* **39**, 168-177.

Seaman, M. N. (2005). Recycle your receptors with retromer. *Trends Cell Biol.* **15**, 68-75.

Seaman, M. N. (2007). Identification of a novel conserved sorting motif required for retromer-mediated endosome-to-TGN retrieval. *J. Cell Sci.* **120**, 2378-2389.

Small, S. A., Kent, K., Pierce, A., Leung, C., Kang, M. S., Okada, H., Honig, L., Vonsattel, J. P. and Kim, T. W. (2005a). Model-guided microarray implicates the retromer complex in Alzheimer's disease. *Ann. Neurol.* **58**, 909-919.

Small, S. A., Kent, K., Pierce, A., Leung, C., Kang, M. S., Okada, H., Honig, L., Vonsattel, J. P. and Kim, T. W. (2005b). Model-guided microarray implicates the retromer complex in Alzheimer's disease. *Ann. Neurol.* **58**, 909-919.

Svitkina, T., Lin, W. H., Webb, D. J., Yasuda, R., Wayman, G. A., Van Aelst, L. and Soderling, S. H. (2010). Regulation of the postsynaptic cytoskeleton: roles in development, plasticity, and disorders. *J. Neurosci.* **30**, 14937-14942.

Temkin, P., Lauffer, B., Jäger, S., Cimermancic, P., Krogan, N. J. and von Zastrow, M. (2011). SNX27 mediates retromer tubule entry and endosome-to-plasma membrane trafficking of signalling receptors. *Nat. Cell Biol.* **13**, 715-721.

van Weering, J. R., Verkade, P. and Cullen, P. J. (2010). SNX-BAR proteins in phosphoinositide-mediated, tubular-based endosomal sorting. *Semin. Cell Dev. Biol.* **21**, 371-380.

Vassar, R. and Kandalepas, P. C. (2011). The β-secretase enzyme BACE1 as a therapeutic target for Alzheimer's disease. *Alzheimers Res. Ther.* **3**, 20.

Vieira, S. I., Rebelo, S., Esselmann, H., Wiltfang, J., Lah, J., Lane, R., Small, S. A., Gandy, S., da Cruz E Silva, E. F. and da Cruz E Silva, O. A. (2010). Retrieval of the Alzheimer's amyloid precursor protein from the endosome to the TGN is S655 phosphorylation state-dependent and retromer-mediated. *Mol. Neurodegener.* **5**, 40.

Vilariño-Güell, C., Wider, C., Ross, O. A., Dachsel, J. C., Kachergus, J. M., Lincoln, S. J., Soto-Ortolaza, A. I., Cobb, S. A., Wilhoite, G. J., Bacon, J. A. et al. (2011). VPS35 mutations in Parkinson disease. *Am. J. Hum. Genet.* **89**, 162-167.

Wang, C. L., Zhang, L., Zhou, Y., Zhou, J., Yang, X. J., Duan, S. M., Xiong, Z. Q. and Ding, Y. Q. (2007). Activity-dependent development of callosal projections in the somatosensory cortex. *J. Neurosci.* **27**, 11334-11342.

Wassmer, T., Attar, N., Harterink, M., van Weering, J. R., Traer, C. J., Oakley, J., Goud, B., Stephens, D. J., Verkade, P., Korswagen, H. C. et al. (2009). The retromer coat complex coordinates endosomal sorting and dynein-mediated transport, with carrier recognition by the trans-Golgi network. *Dev. Cell* **17**, 110-122.

Wen, L., Tang, F. L., Hong, Y., Luo, S. W., Wang, C. L., He, W., Shen, C., Jung, J. U., Xiong, F., Lee, D. H. et al. (2011). VPS35 haploinsufficiency increases Alzheimer's disease neuropathology. *J. Cell Biol.* **195**, 765-779.

Willnow, T. E., Carlo, A. S., Rohe, M. and Schmidt, V. (2010). SORLA/SORL1, a neuronal sorting receptor implicated in Alzheimer's disease. *Rev. Neurosci.* **21**, 315-329.

Xie, Y., Ding, Y. Q., Hong, Y., Feng, Z., Navarre, S., Xi, C. X., Zhu, X. J., Wang, C. L., Ackerman, S. L., Kozlowski, D. et al. (2005). Phosphatidylinositol transfer protein-α in netrin-1-induced PLC signalling and neurite outgrowth. *Nat. Cell Biol.* **7**, 1124-1132.

Yang, P. T., Lorenowicz, M. J., Silhankova, M., Coudreuse, D. Y., Betist, M. C. and Korswagen, H. C. (2008). Wnt signaling requires retromer-dependent recycling of MIG-14/Wntless in Wnt-producing cells. *Dev. Cell* **14**, 140-147.

Zhou, Z., Xie, J., Lee, D., Liu, Y., Jung, J., Zhou, L., Xiong, S., Mei, L. and Xiong, W. C. (2010). Neogenin regulation of BMP-induced canonical Smad signaling and endochondral bone formation. *Dev. Cell* **19**, 90-102.

Zhu, X. J., Wang, C. Z., Dai, P. G., Xie, Y., Song, N. N., Liu, Y., Du, Q. S., Mei, L., Ding, Y. Q. and Xiong, W. C. (2007). Myosin X regulates netrin receptors and functions in axonal path-finding. *Nat. Cell Biol.* **9**, 184-192.

Zimprich, A., Benet-Pagès, A., Struhal, W., Graf, E., Eck, S. H., Offman, M. N., Haubenberger, D., Spielberger, S., Schulte, E. C., Lichtner, P. et al. (2011). A mutation in VPS35, encoding a subunit of the retromer complex, causes late-onset Parkinson disease. *Am. J. Hum. Genet.* **89**, 168-175.